Nanoscale

PAPER

View Article Online
View Journal

Solid-state nanopores and nanopore arrays optimized for optical detection†

Cite this: DOI: 10.1039/c4nr00305e

Furat Sawafta,‡[a] Bason Clancy,‡[b] Autumn T. Carlsen,[c] Martin Huber[b] and Adam R. Hall*[acd]

Received 17th January 2014
Accepted 3rd May 2014

DOI: 10.1039/c4nr00305e

www.rsc.org/nanoscale

While conventional solid-state nanopore measurements utilize ionic current, there is a growing interest in alternative sensing paradigms, including optical detection. However, a limiting factor in the application of optical schemes in particular is the inherent background fluorescence created by the solid-state membrane itself, which can interfere with the desired signal and place restrictions on the fluorophores that can be employed. An ideal device would incorporate a localized reduction in membrane fluorescence using a method that can be integrated easily with the nanopore fabrication process. Here, we demonstrate that in addition to forming nanopores and nanopore arrays, a focused helium ion beam can be used to reduce the fluorescence of a conventional silicon nitride membrane controllably. The reduction in background produces low-fluorescence devices that can be used for optical detection of double-strand DNA, as well as for conventional resistive pulse sensing. This approach is used to identify the translocation of short single-strand DNA through individual nanopores within an array, creating potential for a massively-parallel detection scheme.

Introduction

As single-molecule sensors, solid-state (SS-) nanopores[1] hold great potential in applications ranging from genomic profiling[2,3] to the detection of bioterrorism agents.[4] The approach is elegant in its simplicity: a single, nanometer-scale opening is fabricated in a continuous membrane made of solid-state material (usually silicon nitride). Introduction of ionic solution to either side of the membrane leaves the opening as a narrow passageway through which charged molecules like nucleic acids,[5–7] proteins,[8–10] and solid-state materials[11–13] can be transported using an electric field. Conventionally, these devices rely on ionic current passing through the nanopore as the basis of the measurement; the temporary presence of a single molecule in the opening can alter the transfer of ions significantly through obstruction and other effects.[14] Recently, however, limitations have been identified with this strategy as it pertains to the identification of small molecules or molecular substructure like genetic sequence.[2] Chief among these limitations is the combination of the relatively large membrane thickness (typically >20 nm) and the presence of the access region[15] – a volume sensitive to molecular interactions that reaches a pore radius into the solution at each mouth of the nanopore. As a result, the sensing region is large and cannot be used to resolve small features easily. This has propelled the investigation of alternative detection methods, including the use of graphene as an atomically-thin membrane material with advantageous electrical properties[16–18] and the integration of transverse tunneling electrodes surrounding the pore.[11,19,20]

One approach that is of particular interest is the use of single-molecule fluorescence to perform optical detection of translocations. Here, the passage of fluorescently-labeled molecules through the SS-nanopore is monitored using optical fluorescence imaging of the membrane during the application of a voltage. Optical detection offers the ability to observe molecular translocation directly and thus avoid questions of interpretation that are often encountered with ionic current measurements.[21,22] In addition, a rich assortment of techniques like total internal reflection fluorescence microscopy[23,24] and Förster resonance energy transfer[25] can be integrated with the basic optical measurement technique and can add functionality for measuring positional and structural information with spatial accuracy that can be superior to conventional ionic current measurement.[26,27]

There are several device characteristics that are important in a nanopore optical detection scheme. First, a large range of SS-nanopore diameters should be attainable. Pore diameter has proven an important factor in controlling the translocation

[a]Joint School of Nanoscience and Nanoengineering, University of North Carolina Greensboro, Greensboro, NC 27401, USA

[b]Quantapore Inc., Menlo Park, CA 94025, USA

[c]Department of Biomedical Engineering, Wake Forest University School of Medicine, Winston-Salem, NC 27101, USA

[d]Comprehensive Cancer Center, Wake Forest University School of Medicine, Winston-Salem, NC 27101, USA. E-mail: arhall@wakehealth.edu

† Electronic supplementary information (ESI) available. See DOI: 10.1039/c4nr00305e

‡ Authors contributed equally.

process, both for preventing molecular folding[7] and regulating threading speed.[22,28] Second, large arrays of individual SS-nanopores should be achievable. A major advantage of optical detection in general is the ability to perform measurements in a massively-parallel fashion through simultaneous monitoring of many nanopores. Such a capability is difficult to achieve with conventional ionic current measurement, as individual pores are not individually addressable. Finally, and most critically, the device itself should have low inherent fluorescence. Background fluorescence increases the noise floor of the measurement, making single-molecule detection more challenging and potentially preventing the use of certain fluorophores entirely (see ESI Fig. S2†). For maximum resolution and experimental flexibility, a membrane with little or no fluorescence is ideal.

Of the relatively few reports integrating optical microscopy with SS-nanopore translocations,[26,27,29–31] most have not addressed the issue of membrane fluorescence. Recent work by dela Torre, *et al.*[32] showed that background fluorescence can be reduced using atomic layer deposition of TiO_2 on nanopores formed by focused ion beam. However, this process required multiple fabrication steps and achieved minimum diameters no smaller than ~8 nm. Here, we show that a single fabrication process can address all of the criteria for an optimized SS-nanopore optical detection scheme listed above. We utilize the beam of a commercial helium ion microscope (HIM) to first reduce the fluorescence of a thin silicon nitride (SiN) membrane in a controllable manner and then produce SS-nanopores within that membrane. He^+ ion milling is capable[33] of producing nanopores at high resolution (diameters below 3 nm), either individually or in arbitrarily large arrays. We show that low-fluorescence devices are capable of conventional resistive pulse sensing as well as optical detection of molecular translocations and we demonstrate that large SS-nanopore arrays can be addressed through parallel monitoring.

Results and discussion

SiN membrane fluorescence is thought to be caused by the presence of optically-active defects embedded within the material.[34,35] These radiative centers may be either amorphous[36] or crystalline[37] domains that emit over a range of 400–800 nm. It has been shown previously that a HIM beam at high dose (>10^6 ions per nm^2) is capable of milling through a thin SiN membrane entirely to form a pore[33] and that intermediate doses (>10^4 ions per nm^2) can be used to reduce membrane thickness controllably.[38] However, our previous work has demonstrated[39] that He^+ ions penetrate the membrane easily under typical beam conditions, and so significant effects occur internal to the bulk membrane at energies well below those required to ablate material (*i.e.* the SiN surface binding energy), including atom–atom interaction and implantation. We therefore hypothesize that exposure with a focused He^+ ion beam at low dose (<10^4 ions per nm^2, Fig. 1a) could be used to remove the source of background fluorescence (Fig. 1b) either through ion-induced damage of defects[40,41] or through effects like channeling[42] while leaving the membrane otherwise unaltered.

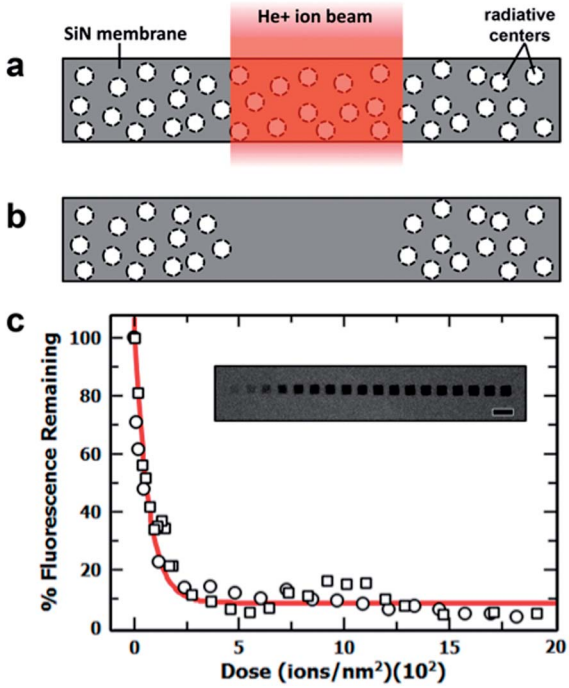

Fig. 1 Helium ion bleaching. (a) A silicon nitride membrane containing defects that act as radiative centers is exposed by a focused He^+ ion beam (red). (b) The beam removes the radiative capacity of these defects and thus their contribution to background fluorescence. (c) Relationship between membrane fluorescence intensity and He^+ ion dose as measured from 500 nm square patterns. Squares and circles are data sets from two separate chips and the solid line is an exponential fit to all data. Inset shows fluorescent image of one sample (circle data points), with dose increasing L–R. Scale bar is 1 μm.

To investigate this, we expose a suspended SiN membrane (30 nm thick) with various doses of He^+ ions and then image the sample with TIRF microscopy (see ESI Fig. S1†). The inset to Fig. 1c shows a typical image, indicating that fluorescence intensity is indeed reduced with increasing amounts of ion exposure. Image analysis can be used to quantify the intensity change relative to the untreated membrane (Fig. 1c), revealing that the fluorescence intensity scales exponentially with He^+ beam dose. At ~300 ions per nm^2, membrane fluorescence is diminished to less than 10% of its initial value and any additional reduction above this dose is not measurable due to the limitations of the detector. We note that this dose is at least an order of magnitude less than the lowest dose investigated previously using a membrane of comparable initial thickness.[39] From these past measurements, we expect that the exposure required here would reduce the average membrane thickness within the exposed region by less than 1 nm. This value is lower than the average roughness of the membrane (typically 2–3 nm), and so we conclude that the low-fluorescence membrane is essentially identical to an untreated membrane.

Having established the efficacy of this technique, we next study quenched SiN as a substrate for optical SS-nanopore measurements. We first expose a 4 μm square region in a SiN membrane with the He^+ ion beam at a dose of ~400 ions

per nm^2 to reduce native fluorescence to a minimal level (Fig. 2a). Directly following this treatment, we expose a spot at the center of the pattern with a dose of 12×10^6 ions per nm^2 in order to produce a single nanopore with a diameter of ~5 nm (see ESI Fig. S1 for example†). We subsequently investigate the passage of a 2.8 kbp dsDNA fragment (derived from λ-phage DNA) through the device. In order to measure translocations both by conventional ionic current and by fluorescence, we end-label the DNA with the fluorophore Cy3. Avoiding intercalating dyes maintains a DNA structure similar to that studied widely elsewhere[5,7,33,43] while providing a fluorescent beacon for optical detection. Fig. 2b shows typical traces of ionic conductance (left) and nanopore fluorescent intensity (right) during application of a 600 mV bias between the two chambers. In the conductance trace, we observe a series of downward spikes with average depth of 1.3 nS, in agreement with past measurements.[5,7,33] In the optical trace, we observe a series of brief increases in fluorescence intensity, each lasting 1–3 video frames (2–6 ms), indicative of the transient presence of a DNA-conjugated fluorophore in the narrow optical sensing region of the SS-nanopore. This dwell time is in agreement with related measurements.[31] We note that our system is not capable of simultaneous measurement, and so individual events cannot be synchronized between optical and electrical signals.[31] In sequential measurements on the same device, we find that the event frequency in both the electrical and the optical signal yields an identical value of 0.45 Hz. Repeating the measurement using unlabeled dsDNA of equivalent length results in events only in the electrical signal and not the optical. However, molecules can occasionally approach the nanopore without necessarily passing through,[21,22,44,45] and so some fraction of the events observed in both the optical and electrical signals could represent non-translocative interactions with the system. Therefore, we suggest only that the fluorescence intensity spikes likely have the same origin as the conductance events. Alternative microscopy techniques[30,46] may be necessary to identify true molecular translocations.

Previous work has demonstrated[33] that He^+ ion milling can be used to form large arrays of individual SS-nanopores with diameters as low as 5 nm. This capability could be exploited to allow parallel optical detection of DNA translocations. However, an aspect that must be considered is how each nanopore in a large array can be localized accurately. Our approach allows this obstacle to be addressed inherently. Because the diameter of the He^+ beam (*i.e.* the width of its Gaussian intensity profile) is larger than the SS-nanopores it produces, the region directly surrounding each pore is exposed to an ion dose that decreases radially from the beam center. As a result, each nanopore should be surrounded by a corona of quenched fluorescence. Such a feature would provide a direct way of locating SS-nanopores optically. To confirm this, we expose an untreated SiN membrane with a range of pore-forming He^+ ion doses and then collect fluorescent images of the sample. A typical image of a 5 × 5 nanopore array is shown in Fig. 3 (inset), where the exposure doses range from $\sim 1 \times 10^7$ to 11×10^7 ions per nm^2. As expected, we find that each nanopore is marked by a discrete region of reduced fluorescence. In order to analyze these data, we consider the diameter of each spot to be the width of a Gaussian fit to its cross-sectional intensity profile. We find that the diameter of the quenched region varies logarithmically with the He^+ ion dose (Fig. 3). Practically, the observation verifies that SiN fluorescence is quenched strongly at the location of the SS-nanopore as an intrinsic effect of our fabrication process.

We can therefore investigate He^+ ion-milled nanopore arrays as the basis of a parallel optical detection technique. To do this, we fabricate a 20 × 20 array of individual pores with diameters of ~5 nm in a SiN membrane that has been treated as described above to reduce background fluorescence to ~20% of its initial value (see Fig. 1c). Fig. 4a shows a TIRF optical micrograph of the device, in which the individual SS-nanopores can be

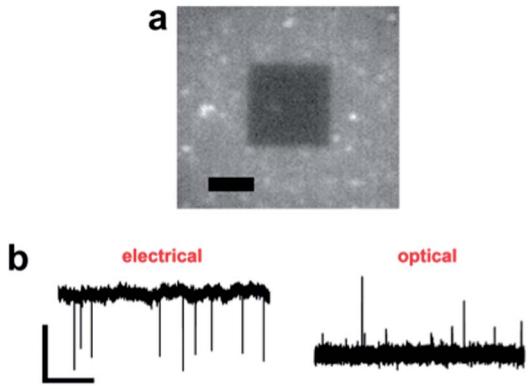

Fig. 2 Electrical and optical detection of DNA translocations. (a) Optical image of a He^+ ion-bleached square containing a single SSnanopore with diameter 5 nm. Scale bar is 2 μm. (b) Typical raw traces taken with the device, showing Cy3-labeled DNA translocation events using both conventional ionic conductance (left) and fluorescence intensity (right). Scale bar applies to both traces, with a horizontal scale of 5 s and a vertical scale of 1 nS (electrical) and 25 a.u. of gray scale (optical).

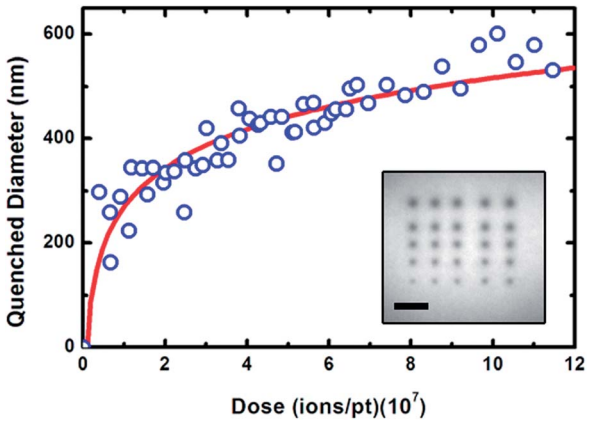

Fig. 3 Fluorescence quenching around individual SS-nanopores. The diameter of fluorescence quenching around individual SS-nanopores on an untreated silicon nitride membrane plotted against the He^+ ion exposure dose of the pore. Solid line is a logarithmic fit to the data. Inset shows a typical fluorescence image of a 25-pore array with He^+ ion exposure doses ranging from $\sim 1 \times 10^7$ (lower left) to 11×10^7 (upper right) ions per nm^2. Scale bar is 2 μm.

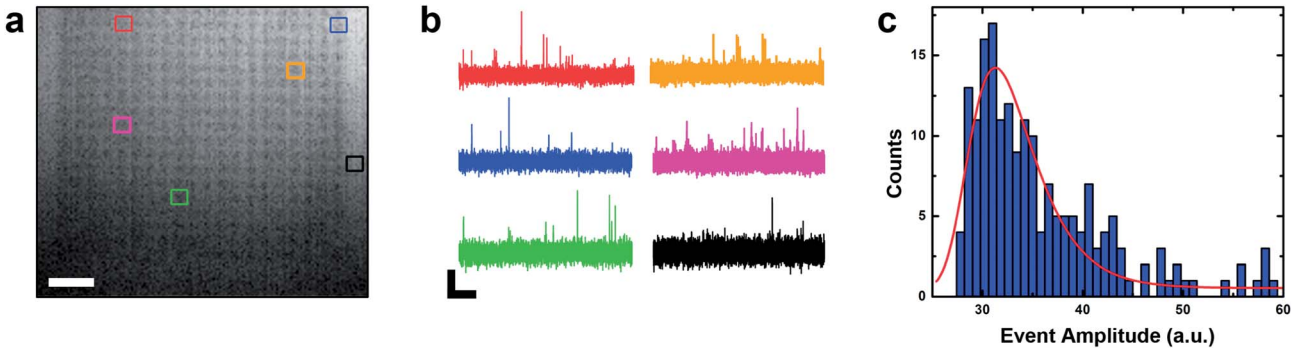

Fig. 4 Parallel optical detection of DNA translocations. (a) Fluorescence image of a 20 × 20 array of ~5 nm diameter SS-nanopores formed in a SiN membrane with locally-quenched background fluorescence. Image is an average of 100 video frames and contrast has been adjusted for clarity. Scale bar is 2.5 μm. (b) Raw fluorescence intensity traces measured simultaneously from video of Cy3-labeled ssDNA translocations through five typical nanopores (each outlined in corresponding color) within the array. The black trace is measured on a region of the membrane with reduced-fluorescence proximal to the array (outlined in black), indicating very few spikes. Scale bar is 0.5 s (horizontal) and 30 a.u. (vertical). (c) Histogram of optical event amplitudes ($n = 191$) measured at the locations of individual nanopores within the array. The red line is a log-normal fit to the data.

resolved as small dark spots. On the far side of the membrane, we introduce 55-base long single-strand (ss) DNA molecules, each containing 3 Cy3 labels and collect video while applying 1 V across the device. Short, homopolymeric ssDNA oligonucleotides are used here in order to avoid clogging and to demonstrate the efficacy of the approach at resolving small molecules. To our knowledge, ssDNA translocations through SS-nanopores have not been detected using an optical approach previously. In the video, we observe transient increases in brightness at the locations of the SS-nanopores, similar to what was seen in the prior single-pore case. However, we are now able to monitor translocations through individual pores within the array simultaneously. Fig. 4b shows fluorescent intensity traces for five representative nanopores within the array, each yielding a series of transient spikes in image brightness that denote the passage of individual molecules. We attribute the broad distribution of fluorescence event amplitudes (Fig. 4c) to the video capture rate (675 Hz), which is low compared to the speed of the DNA translocation. This disparity creates variation in apparent fluorophore brightness since a molecule can reside at different positions relative to the focal plane during image capture.

Free diffusion of a fluorophore into the focal volume of the microscope can also produce a transient increase in fluorescence intensity. Therefore, it is possible that some optical events may be attributed to molecules drifting through the area of interest. In order to explore this possibility, we perform an additional analysis on the data shown in Fig. 4. Considering several individual SS-nanopores from within the array ($n = 32$), we measure an event rate of 0.27 Hz. Repeating the same measurement at 12 (partially quenched) areas proximal to the array but not at the location of a pore (*c.f.* black trace in Fig. 4b), we observe that there is a low but measurable event rate (0.03 Hz). These events are likely caused by random diffusion of translocated material into the focal region during the measurement, and are comparable to actual translocations in terms of amplitude. However, the event rate measured at the membrane is roughly an order of magnitude lower than that measured at the SS-nanopore locations, and so we estimate that no more than 10% of events detected optically at the location of a nanopore could be attributed to diffusion of material through the field of view. Thus, the vast majority of fluorescence intensity spikes measured in the nanopore array correspond to translocation events or stochastic interactions with the sensing region (see discussion above). Synchronous optical and electrical measurements should be able to differentiate non-translocative interactions more fully.

Conclusions

We have shown that a focused He^+ ion beam is able to reduce the fluorescence of a SiN membrane in a manner that integrates seamlessly with the SS-nanopore fabrication process. We propose that the mechanism of this effect is tied to ion beam-induced damage to optically-active defects within the SiN. Background fluorescence can be reduced or removed accurately using arbitrary lithographic patterning. We have also demonstrated that quenched SS-nanopores can be used for both resistive-pulse sensing as well as optical identification of DNA translocations. Finally, we showed that the area directly surrounding He^+ ion-milled SS-nanopores is quenched intrinsically by the beam, resulting in an optically-addressable device with no further fabrication steps. This permitted the study of SS-nanopore arrays that could be addressed by TIRF imaging. As the number of parallel nanopores is increased, the contribution of a single molecular translocation to the electrical signal becomes insignificant and therefore increasingly difficult to resolve. The fluorescence intensity, however, remains unaffected for arbitrarily large numbers of individual SS-nanopores. As a result, we were able to demonstrate for the first time that ssDNA translocations through individual SS-nanopores within a large (20 × 20) array can be detected with a parallel optical measurement.

Our approach makes the fabrication of SS-nanopores and nanopore arrays for optical applications fast and accurate. These devices may find specific near-term use in genetic

sequencing applications that rely on fluorescent interactions for their central measurement.[26,27] The controlled, lithographic reduction of substrate fluorescence may also find use in a variety of applications, including distance calibration in fluorescence microscopy and optoelectronics.

Methods

SS-nanopore fabrication

Si chips each supporting a free-standing SiN membrane 30 nm thick were purchased commercially (Protochips, Raleigh, NC) and used as delivered. Prior to use, all Si chips were cleaned with acetone and ethanol and dried under a nitrogen stream, after which they were exposed to oxygen plasma (10 W) for 3 minutes in the antechamber of the helium ion microscope (Zeiss Orion Plus, Carl Zeiss, Peabody, MA) before being moved into the main chamber of the microscope for treatment. The ion beam current was adjusted to 5–6 pA through a 20 μm aperture and beam shape and focus were optimized at a spot near the suspended SiN membrane directly prior to membrane exposure. Fluorescence quenching was performed by a computer-controlled exposure of a patterned square with a set He^+ ion dose. SS-nanopores were formed by exposing a single spot on the membrane for a prescribed amount of time. Diameter was determined by transmission helium ion imaging of a calibration array formed on a membrane from the same batch. SS-nanopore diameters were confirmed using the measured *I–V* characteristics of a given device and a geometric model.[14] For arrays, all pores were considered parallel resistors and the *I–V* method yielded the mean nanopore diameter.

Biomolecule preparation

For the data in Fig. 2, λ-phage DNA (New England Biolabs, Ipswitch, MA) was digested with SfoI which results in two fragments with lengths of 45 679 bp and 2823 bp, respectively. The 2823 bp fragment was gel-purified and end-labeled with a single Cy3 fluorophore using terminal transferase and Cy3-dCTP. Excess Cy3-dCTP was removed by dialyzation against 1X PBS overnight at ambient temperature. This procedure has the potential to add multiple modified nucleotides to the 3′ terminus, but the bulky fluorescent group limits incorporation efficiency. Only 1–3 fluorophores are observed when investigating bleaching behavior of labeled DNA with single-molecule imaging. For the data shown in Fig. 4, custom 55-base ssDNA oligonucleotides (Integrated DNA Technologies, Coralville, IA) were used, each containing 3 Cy3 fluorophores with the following sequence: 5′-Cy3-T_{20}-Cy3-T_{20}-Cy3-T_{15}-3′.

SS-nanopore measurements

The Si chip containing the target SS-nanopore or pore array was loaded into a custom flow cell with PDMS gaskets. The separation between the chip and the bottom surface of the flow cell is 5–10 μm, allowing high-NA optical imaging of the SiN membrane. During optical measurements, the TIRF excitation beam is delivered to the SiN membrane taking into account the diffractive index of the fluid in the lower chamber, resulting in total reflection of the laser at the interface of the SiN membrane with the upper fluid chamber. All translocation experiments were performed in solvent conditions of 1 M KCl, 10 mM tris, and 1 mM EDTA. Electrical measurements were collected *via* a patch clamp amplifier (Axopatch 200B) using Ag/AgCl electrodes at 100 kHz and low-pass filtered at 1 kHz.

Fluorescent imaging

Images for Fig. 1 were captured on an inverted optical microscope (Zeiss Observer A1) with a filter set of 488 nm (excitation) and 515 nm (emission). This is near the maximum expected intensity for SiN.[36,37] All further imaging was performed on a custom inverted microscope with a 60× TIRF objective (Olympus APON OTIRF, NA 1.49) and a filter set of 532 nm (excitation) and 561 nm (emission), optimized for the target fluorophore (Cy3). The excitation source was a diode-pumped solid-state laser (4 mW, Laserglow Technologies LRS-0532) and video was collected with a CMOS camera (Hamamatsu ORCA-Flash 4.0) at a rate of 500 Hz for Fig. 2 and 675 Hz for Fig. 4. Optical translocation traces were produced by plotting the mean gray value brightness of the 5 × 5 pixel region surrounding a single nanopore over time. Image and video analysis were performed using ImageJ software.[47]

Acknowledgements

We acknowledge valuable discussions with J. Yang. ARH acknowledges start-up funding from the Wake Forest University School of Medicine.

Notes and references

1 C. Dekker, *Nat. Nanotechnol.*, 2007, **2**, 209–215.
2 D. Branton, D. W. Deamer, A. Marziali, H. Bayley, S. A. Benner, T. Butler, M. Di Ventra, S. Garaj, A. Hibbs, X. Huang, S. B. Jovanovich, P. S. Krstic, S. Lindsay, X. S. Ling, C. H. Mastrangelo, A. Meller, J. S. Oliver, Y. V. Pershin, J. M. Ramsey, R. Riehn, G. V. Soni, V. Tabard-Cossa, M. Wanunu, M. Wiggin and J. A. Schloss, *Nat. Biotechnol.*, 2008, **26**, 1146–1153.
3 M. Wanunu, *Phys. Life Rev.*, 2012, **9**, 125–158.
4 A. H. Liu, Q. T. Zhao and X. Y. Guan, *Anal. Chim. Acta*, 2010, **675**, 106–115.
5 J. L. Li, M. Gershow, D. Stein, E. Brandin and J. A. Golovchenko, *Nat. Mater.*, 2003, **2**, 611–615.
6 G. M. Skinner, M. van den Hout, O. Broekmans, C. Dekker and N. H. Dekker, *Nano Lett.*, 2009, **9**, 2953–2960.
7 A. J. Storm, J. H. Chen, H. W. Zandbergen and C. Dekker, *Phys. Rev. E*, 2005, **71**, 051903.
8 M. Firnkes, D. Pedone, J. Knezevic, M. Doeblinger and U. Rant, *Nano Lett.*, 2010, **10**, 2162–2167.
9 A. P. Han, G. Schurmann, G. Mondin, R. A. Bitterli, N. G. Hegelbach, N. F. de Rooij and U. Staufer, *Appl. Phys. Lett.*, 2006, **88**, 093901.
10 C. Plesa, S. W. Kowalczyk, R. Zinsmeester, A. Y. Grosberg, Y. Rabin and C. Dekker, *Nano Lett.*, 2013, **13**, 658–663.

11 B. C. Gierhart, D. G. Flowitt, S. J. Chen, Z. Zhu, D. E. Kotecki, R. L. Smith and S. D. Collins, *Sens. Actuators, B*, 2008, **132**, 593–600.
12 A. R. Hall, J. M. Keegstra, M. C. Duch, M. C. Hersam and C. Dekker, *Nano Lett.*, 2011, **11**, 2446–2450.
13 A. S. Prabhu, T. Z. N. Jubery, K. J. Freedman, R. Mulero, P. Dutta and M. J. Kim, *J. Phys.: Condens. Matter*, 2010, **22**, 454107.
14 R. M. M. Smeets, U. F. Keyser, D. Krapf, M. Y. Wu, N. H. Dekker and C. Dekker, *Nano Lett.*, 2006, **6**, 89–95.
15 J. E. Hall, *J. Gen. Physiol.*, 1975, **66**, 531–532.
16 S. Garaj, W. Hubbard, A. Reina, J. Kong, D. Branton and J. A. Golovchenko, *Nature*, 2010, **467**, 190.
17 C. A. Merchant, K. Healy, M. Wanunu, V. Ray, N. Peterman, J. Bartel, M. D. Fischbein, K. Venta, Z. T. Luo, A. T. C. Johnson and M. Drndic, *Nano Lett.*, 2010, **10**, 2915–2921.
18 G. F. Schneider, S. W. Kowalczyk, V. E. Calado, G. Pandraud, H. W. Zandbergen, L. M. K. Vandersypen and C. Dekker, *Nano Lett.*, 2010, **10**, 3163–3167.
19 Z. J. Jiang, M. Mihovilovic, J. Chan and D. Stein, *J. Phys.: Condens. Matter*, 2010, **22**, 454114.
20 E. S. Sadki, S. Garaj, D. Vlassarev, J. A. Golovchenko and D. Branton, *J. Vac. Sci. Technol., B*, 2011, **29**, 053001.
21 M. van den Hout, V. Krudde, X. J. A. Janssen and N. H. Dekker, *Biophys. J.*, 2010, **99**, 3840–3848.
22 M. Wanunu, J. Sutin, B. McNally, A. Chow and A. Meller, *Biophys. J.*, 2008, **95**, 4716–4725.
23 D. Axelrod, T. P. Burghardt and N. L. Thompson, *Annu. Rev. Biophys. Bioeng.*, 1984, **13**, 247–268.
24 W. E. Moerner and D. P. Fromm, *Rev. Sci. Instrum.*, 2003, **74**, 3597–3619.
25 E. A. Jares-Erijman and T. M. Jovin, *Nat. Biotechnol.*, 2003, **21**, 1387–1395.
26 B. McNally, A. Singer, Z. L. Yu, Y. J. Sun, Z. P. Weng and A. Meller, *Nano Lett.*, 2010, **10**, 2237–2244.
27 G. V. Soni and A. Meller, *Clin. Chem.*, 2007, **53**, 1996–2001.
28 U. Mirsaidov, J. Comer, V. Dimitrov, A. Aksimentiev and G. Timp, *Nanotechnology*, 2010, **21**, 395501.
29 P. Chen, J. J. Gu, E. Brandin, Y. R. Kim, Q. Wang and D. Branton, *Nano Lett.*, 2004, **4**, 2293–2298.
30 V. Kurz, E. M. Nelson, J. Shim and G. Timp, *ACS Nano*, 2013, **7**, 4057–4069.
31 G. V. Soni, A. Singer, Z. L. Yu, Y. J. Sun, B. McNally and A. Meller, *Rev. Sci. Instrum.*, 2010, **81**, 014301.
32 R. dela Torre, J. Larkin, A. Singer and A. Meller, *Nanotechnology*, 2012, **23**, 385308.
33 J. Yang, D. C. Ferranti, L. A. Stern, C. A. Sanford, J. Huang, Z. Ren, L.-C. Qin and A. R. Hall, *Nanotechnology*, 2011, **22**, 285310.
34 S. V. Deshpande, E. Gulari, S. W. Brown and S. C. Rand, *J. Appl. Phys.*, 1995, **77**, 6534–6541.
35 M. H. Wang, D. S. Li, Z. Yuan, D. R. Yang and D. L. Que, *Appl. Phys. Lett.*, 2007, **90**, 131903.
36 N. M. Park, C. J. Choi, T. Y. Seong and S. J. Park, *Phys. Rev. Lett.*, 2001, **86**, 1355–1357.
37 B. H. Kim, C. H. Cho, T. W. Kim, N. M. Parka, G. Y. Sung and S. J. Park, *Appl. Phys. Lett.*, 2005, **86**, 222101.
38 M. M. Marshall, J. Yang and A. R. Hall, *Scanning*, 2012, **34**, 101–106.
39 A. R. Hall, *Microsc. Microanal.*, 2013, **19**, 740–744.
40 S. Cheylan, N. Langford and R. G. Elliman, *Nucl. Instrum. Methods Phys. Res., Sect. B*, 2000, **166**, 851–856.
41 B. Schmidt, A. Mucklich, L. Rontzsch and K. H. Heinig, *Nucl. Instrum. Methods Phys. Res., Sect. B*, 2007, **257**, 30–32.
42 L. G. Jacobsohn, B. L. Bennett, D. W. Cooke, R. E. Muenchausen and M. Nastasi, *J. Appl. Phys.*, 2005, **97**, 033528.
43 A. J. Storm, C. Storm, J. H. Chen, H. Zandbergen, J. F. Joanny and C. Dekker, *Nano Lett.*, 2005, **5**, 1193–1197.
44 S. W. Kowalczyk and C. Dekker, *Nano Lett.*, 2012, **12**, 4159–4163.
45 D. M. Vlassarev and J. A. Golovchenko, *Biophys. J.*, 2012, **103**, 352–356.
46 V. V. Thacker, S. Ghosal, S. Hernandez-Ainsa, N. A. W. Bell and U. F. Keyser, *Appl. Phys. Lett.*, 2012, **101**, 223704.
47 C. A. Schneider, W. S. Rasband and K. W. Eliceiri, *Nat. Methods*, 2012, **9**, 671–675.

